01 Jan 2007

Wetting Kinetics of a Thin Film Evaporating in Air

S. Saritha

Partho Neogi

Missouri University of Science and Technology, neogi@mst.edu

Wetting kinetics of a thin film evaporating in air

S. Saritha and P. Neogi[a)]
Chemical and Biological Engineering, University of Missouri-Rolla,[b)] *Rolla, Missouri 65409-1230, USA*

(Received 18 June 2007; accepted 24 October 2007; published online 28 November 2007)

The conservation equation and the equations of motion are solved for a case where a thin liquid film moves out of a slot onto a horizontal surface. The liquid is allowed to evaporate into air. The evaporation process is taken to be isothermal. Lubrication theory approximation is used where only the tangential velocity and its dependence only in the normal direction are considered. The dynamics of thin films includes the use of disjoining pressure for a pure liquid and where there is a dissolved polymer. The results show that evaporation is quicker than film thinning such that a spreading regime dominated by the effects of disjoining pressure is never achieved. However, unlike the cases of pinning studied so far, there is no singularity in the evaporative flux near the contact line because of the use of disjoining pressure on evaporation. It is also observed that a balance between the rate of viscous dissipation and surface work is able to quantify the steady state contact angle. Consequently, a more macroscopic (and quantitative) description of contact line can be found that avoids the singularities discussed earlier and also the detailed calculations shown here. However, the detailed calculations are necessary to make the above point. © *2007 American Institute of Physics*.
[DOI: 10.1063/1.2815737]

I. INTRODUCTION

Consider a drop of liquid lying on a horizontal solid surface where the ambient fluid is air. The line common to the three phases is the contact line, and the angle that the liquid-air interface makes on the solid surface is the contact angle. Theory shows that the evaporation rate under air at the contact line is infinite.[1–5] The evaporative flux at the liquid-air interface is perpendicular to the interface and remains nonzero in the limit that the contact line is approached traveling along the interface. In contrast, the flux at the solid-air interface remains zero when the contact line is approached traveling along this interface. It can be argued then, that the flux there is two-valued and its gradient infinite. However, the special features that need to be considered near a contact line such as the equilibrium contact angle and the disjoining pressure are unaccounted for in most analyses. The steep rise in evaporation rate near the contact line was first reported by Renk and Wayner[6] and what has turned out to be its remedy in a model was arrived at by Moosman and Homsy.[7] The local mass transfer coefficient may show changes. Nevertheless, an average mass transfer coefficient k_L can be defined in the region where such changes take place. This problem with concurrent heat, mass, and momentum transfer is complex. Simplification is made by confining evaporation to be isothermal, thus eliminating the heat transfer, and which is realized when there is no heat source and the latent heat of vaporization is negligible. Another feature that some investigators assume is a lack of local equilibrium at the evaporating interface.[8–10] However, this effect is not expected to be significant unless the ambient fluid is at very low pressures,[11] which will not be considered here.

The main feature of interest here is that the experimental observations indicate that the contact line for an evaporating drop of a nonwetting liquid is often pinned: there is no spreading and the contact angle decreases with time. The Marangoni effect due to the surface tension gradients is argued to be responsible.[5] No Marangoni effect is expected under isothermal conditions for pure liquids (or for equilibrated mixtures).

We study below a contact line where disjoining pressure and its effect on mass transfer and fluid flow are included. Evaporation is assumed to be isothermal. We know that transport singularities can be eliminated, but do not know beforehand if the rate of evaporation can balance the rate of wetting to lead to pinning. The liquids are wetting or nearly wetting, which too is a significant departure as most investigations deal with nonwetting liquids.

Two different disjoining pressures are used here as body forces as functions of local film thickness h:

$$\Pi = \frac{A_{\mathrm{H}}}{12\pi h^3}, \tag{1}$$

$$\Pi = \frac{A_{\mathrm{H}}}{12\pi h^3} - \frac{RT\phi_\infty \rho_p}{M} N \left(\frac{b}{h}\right)^{5/3} e^{-N(b/h)^{5/3}}. \tag{2}$$

The first equation represents the disjoining pressure due to Hamaker interaction alone, while the second includes that due to the presence of a polymer in the liquid. The volume fraction of the polymer in the main drop is ϕ_∞, the density of the polymer ρ_p, the number of steps in the polymer N, the step size b, and the molecular weight of the monomer M. For Hamaker constant $A_{\mathrm{H}} > 0$ assumed here, Eq. (1) represents a wetting liquid. ϕ_∞ times the exponential is the actual polymer concentration in the film. Equation (2) represents a partially wetting liquid. Whereas the form in Eq. (1) cannot

[a)]Electronic mail: neogi@umr.edu.
[b)]Missouri University of Science and Technology from January 7, 2008.

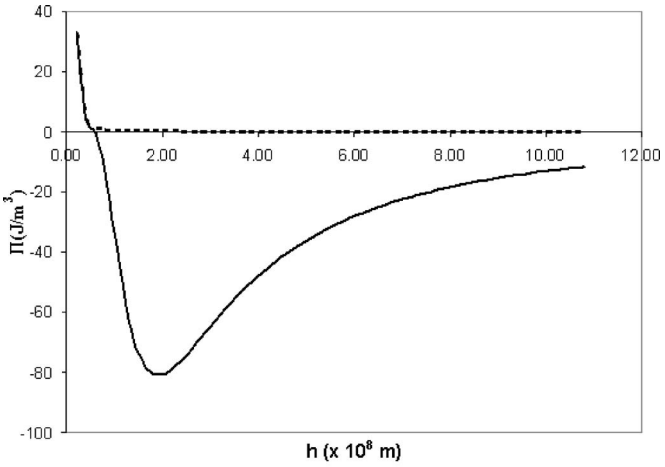

(a)

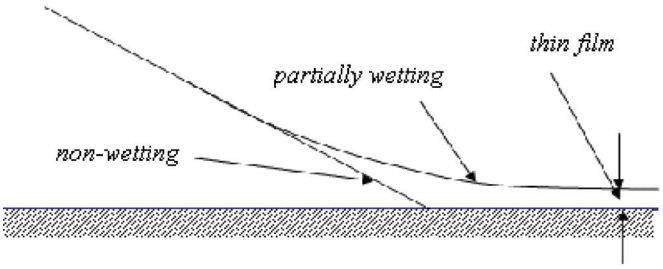

(b)

FIG. 1. (a) Schematic view of disjoining pressures given in Eq. (1), which is always positive, and Eq. (2), which has significant negative portions at large film thickness h. (b) Expected equilibrium film profiles for the two disjoining pressures. For the disjoining pressure given by Eq. (1), no equilibrium is possible, a thin film of constant thickness (including zero thickness) is formed at large times. For the case described by Eq. (2), a wedge ends in a film of constant thickness. The wedge angle is the equilibrium contact angle.

equilibrate and thus represents a wetting liquid, the form given by Eq. (2) can.[12] The equilibrium profile in the vicinity of the contact line is that of a wedge of angle λ, which tapers into a thin film of constant thickness $\hat{h}$. Now, λ is identified as the equilibrium contact angle by Derjaguin-Frumkin equation[13,14]

$$\cos\lambda = 1 + \frac{1}{\gamma}\int_{\hat{h}}^{\infty} \Pi(h)dh, \tag{3}$$

where $\Pi(\hat{h})=0$ for a wedge. Thus, the long time behaviors of the two are different. Sketches of the disjoining pressures are shown in Fig. 1(a) and the expected profiles at equilibrium in Fig. 1(b). It is evident from the figures that the disjoining pressure given by Eq. (2) leads to a profile at equilibrium that has no contact line and the contact angle is defined at sufficient distance above the solid surface.

Use of the Boltzmann factor in Eq. (2) gives rise to a decrease in the local concentration ϕ from the bulk value ϕ_∞ with decreasing film thickness. However, it also ensures that the chemical potential remains the same to some approximation.[15] As a result, an assumption can be made that no Marangoni effect will arise due to changes in concentrations when the chemical potentials do not change.

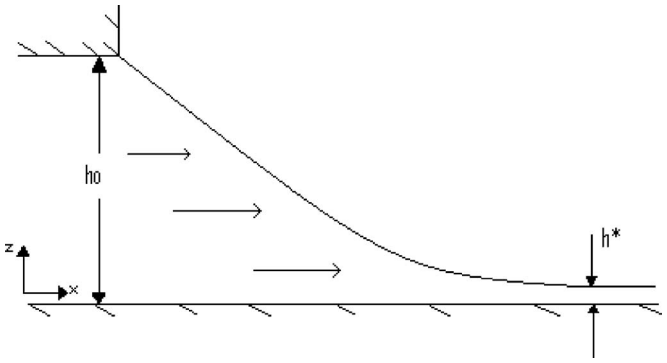

FIG. 2. Schematic view of the spreading thin film. Coordinate system and key parameters are indicated.

II. FORMULATION

Liquid emerges from a slit and flows on the lower surface as shown in Fig. 2 along with the coordinate system. The slit heights used are 100 and 25 nm, where 100 nm is the film thickness for which the disjoining pressure becomes negligible. Since the film is thin and flat and spreads slowly, lubrication theory approximation is used. Here, only the tangential velocity v_x is considered and it is assumed that it varies mainly in the normal direction, z. The equations of motion become

$$0 = \mu\frac{\partial^2 v_x}{\partial z^2} - \frac{\partial(p+\Phi)}{\partial x}, \tag{4}$$

$$0 = \frac{\partial(p+\Phi)}{\partial z}, \tag{5}$$

where p is the Laplace pressure and Φ is the excess potential. The boundary conditions are

$$v_x = 0 \quad \text{at } z = 0, \tag{6}$$

$$\frac{\partial v_x}{\partial z} = 0 \quad \text{at } z = h(x), \tag{7}$$

$$p = -\gamma\frac{\partial^2 h}{\partial x^2} \quad \text{at } z = h(x), \tag{8}$$

$$\Phi = -\Pi(h) \quad \text{at } z = h(x), \tag{9}$$

leading to the tangential velocity averaged over the local thickness

$$\langle v_x\rangle = -\frac{h^2}{3\mu}\frac{\partial}{\partial x}\left(-\gamma\frac{\partial^2 h}{\partial x^2} - \Pi\right). \tag{10}$$

The continuity equation becomes

$$\frac{\partial h}{\partial t} = -\frac{\partial(h\langle v_x\rangle)}{\partial x} - Q(h), \tag{11}$$

where

$$Q = \frac{k_L p_s'(1-\phi)}{\rho_L RT},$$

where k_L is the mass transfer coefficient, ρ_L is the density of the liquid, γ is the surface tension, and R is the universal gas constant. The last term on the right-hand side of Eq. (11) is due to evaporation. The ideal gas law has been used to obtain the concentration of the vapor in the gas phase at the interface. Ideal solution behavior has been used to include the effect of polymer on the vapor pressure. As mentioned earlier, the system is isothermal at temperature T. The saturated vapor pressure of pure liquid at this temperature is p_s, different from p_s' used in Eq. (11), because the total pressure in the liquid has altered because of the Laplace pressure and the disjoining pressure. Thermodynamic considerations are used to relate the two:

$$p_s' = p_s \exp\left\{-\frac{1}{RT\rho_L}\left(\gamma\frac{\partial^2 h}{\partial x^2} + \Pi\right)\right\}. \tag{12}$$

Note that p_s' becomes zero at the contact line of thickness $h=0$. It is described below that we go down in thickness to only h^*. However, this h^* is very small and of the order of molecular dimensions. As a result the saturated vapor pressure falls to negligible values in the immediate vicinity of the contact line. Thus, the fact that the evaporative flux reaches a value of zero at the contact line, eliminates the contact line singularity discussed earlier. Substituting Eq. (12) into Eq. (11) and nondimensionalizing, we get

$$\frac{\partial H}{\partial T} = -\frac{1}{R^2}\frac{\partial}{\partial X}\left[\frac{H^3}{3}\frac{\partial}{\partial X}\left\{\frac{1}{R^2}\frac{\partial^2 H}{\partial X^2} + \bar{\Pi}\right\}\right] - \bar{Q}, \tag{13}$$

where $H=h/h_0$, $X=x/x_0$, $R=x_0/x_0(0)$, $T=[\gamma x_0^2(0)/\mu h_0^3]t$, $\bar{Q}=[\mu x_0^4(0)/h_0^4\gamma]Q$, $\bar{\Pi}=[x_0^2(0)/\gamma h_0]\Pi$. (The incorrectly stated dimensionless group representing T in Saritha *et al.*[12] has been corrected here.)

Equation (13) is subject to boundary conditions that

$$h = h^* \quad \text{at } x = x_o - \ell, \tag{14}$$

$$\frac{\partial h}{\partial x} = 0 \quad \text{at } x = x_o - \ell, \tag{15}$$

$$h = h_0 \quad \text{at } x = 0, \tag{16}$$

$$\frac{\partial^2 h}{\partial x^2} = 0 \quad \text{at } x = 0. \tag{17}$$

The rate of spreading is determined from

$$\langle v_x \rangle_{x=x_o} = \frac{dx_o}{dt}. \tag{18}$$

However, the calculations need to be stopped before the contact line $h=0$ is approached to avoid the contact line singularity. For convenience with the numerical scheme used to solve this problem, the cutoff (ℓ) is defined along x and not in h. The numerical method used has been discussed earlier.[12,16] We have used finite differences. The equations are fourth order and show large problems with instability. Hopscotch is used to decrease this problem, but increasing step sizes in time also increases the error. The step size was initially chosen to be 10^{-9}, but was slowly increased to 10^{-3}.

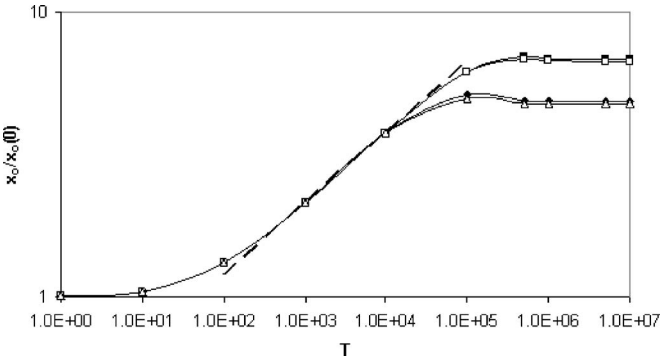

FIG. 3. The extents spread $R=x_o/x_o(0)$ have been shown for the two cases of $h_o=100$ nm (white squares) and $h_o=25$ nm (solid black squares). The corresponding two cases without polymer are shown in solid black triangles ($h_o=25$ nm) and white triangles ($h_o=100$ nm). The dashed line represents the asymptotic 1/4 slope, which is an indication of surface tension driven flow. The white and the black points are almost coincident.

The parameters are obtained by taking the pure liquid to be toluene and the solution to be polystyrene of molecular weight 45 000 in toluene. All other parameters have been taken from Ybarra *et al.*[15] and are $\rho_p=0.8$ g/cm^3, $b=5$ nm, and for the solvent $M=104$. The volume fraction of the polymer in the reservoir is $\phi_\infty=0.05$. To calculate k_L, we use the analogy that

$$\frac{\mathrm{Sh}}{\mathrm{Nu}} = \left(\frac{\mathrm{Sc}}{\mathrm{Pr}}\right)^{2/3}, \tag{19}$$

where Sh is the Sherwood number, Nu the Nusselt number, Sc the Schmidt number, and Pr the Prandtl number. In addition, the fact that the heat transfer coefficient in Nu for air is almost constant at 12 W/(m^2 K) has been used. This provides an estimate for k_L and the main feature studied here; the effects of curvature and disjoining pressure on mass fluxes are felt through their effect on the saturated vapor pressure [Eq. (12)] and the definition of Q following Eq. (11).

III. RESULTS AND DISCUSSION

The distances spread have been plotted as functions of time in Fig. 3. The two cases of liquid with and without polymer are indistinguishable. Steady state is reached in all cases. This is a new result. The fact that the disjoining pressures do not matter is not surprising. At short times, the films are thick and Laplace pressure dominates as the driving force. At large times, the films thin down and the disjoining pressure dominates the spreading rates.[12,16] However, the transition occurs at extremely large times. We find that phenomena such as evaporation come into effect well before the transition to disjoining pressure driven flows comes into effect. This means that emerging thin films are evaporated off and steady state is reached. Earlier investigators[17,18] have found this to be sometimes the case when the substrate is heated, which is a situation where the thin film is more likely to be evaporated off. They have many features besides the nonisothermal condition in their model, such as that the equi-

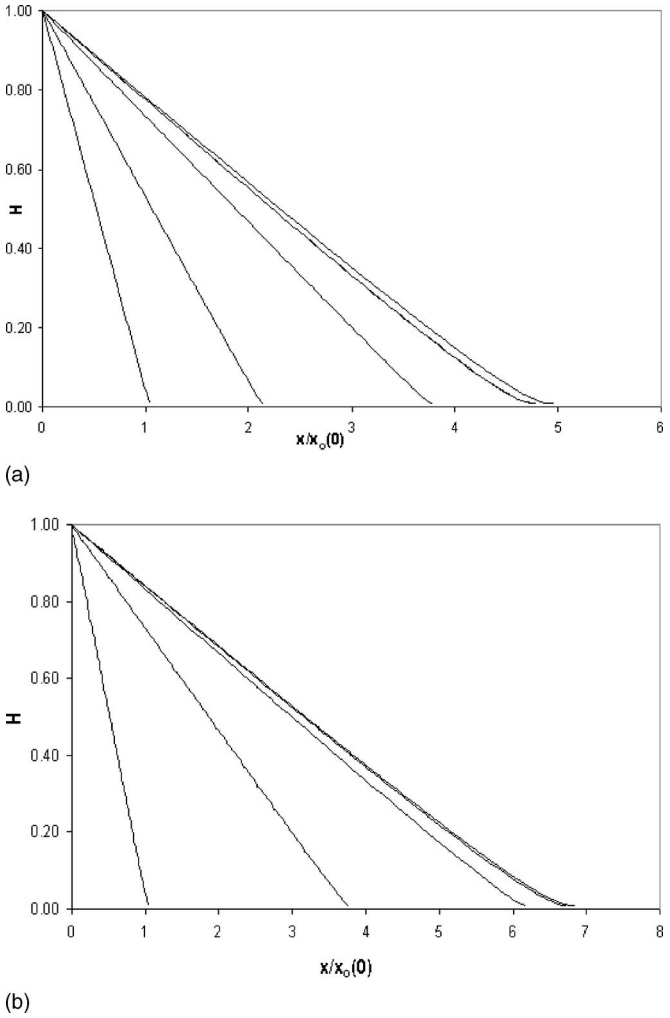

FIG. 4. (a) The film profiles have been shown for the case when $h_o=25$ nm in the absence of polymer. From left to right, the plots are shown at dimensionless times $T=1\times10^3$, 1×10^4, 1×10^5, 5×10^9, 5×10^5. (b) The film profiles have been shown for the case when $h_o=100$ nm in the absence of polymer. From left to right, the plots are shown at dimensionless times $T=1\times10^1$, 1×10^4, 1×10^5, 5×10^5, 1×10^6. The cases with polymer are identical to those above.

librium relation Eq. (12) is linearized. Local nonequilibrium at the interface and Marangoni effect are also included, neither of which applies here. Consequently, comparing their results to ours is difficult.

In Fig. 4, the profiles for the two cases of 25 and 100 nm slit width are shown at different times. Only the cases with no polymer are shown because those with polymer are identical at this scale. The profiles shown at the largest time are such that there is no change in shape at later times; that is, they have reached steady state. It is striking that all profiles, particularly at the steady state, are essentially given by equations of straight lines. It means that at steady state, a contact angle θ (the slope of this line) can be defined/measured, which is not related to the equilibrium contact angle. The measured contact angles are transport dependent. For Figs. 4(a) (25 nm slit) and 4(b) (100 nm slit), they are 3° and 2.25°, respectively.

To understand these, consider the geometry used by de Gennes[19] to quantify the apparent dynamic contact angles.

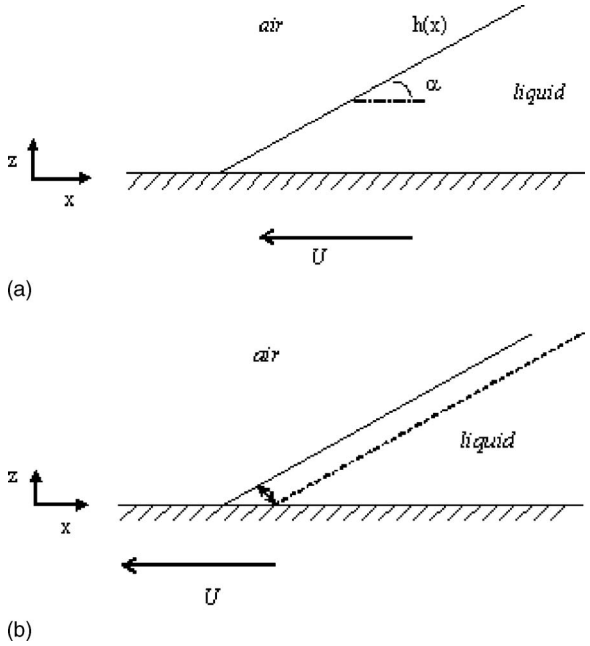

FIG. 5. (a) Schematic view of a liquid wedge on a horizontal solid surface. The flat plate is dragged forward with a velocity U. (b) Schematic view of a liquid wedge evaporating on a horizontal solid surface. The flat plate is dragged forward with a velocity U. The dashed line represents the liquid wedge after time Δt.

A liquid wedge on a horizontal solid surface will wet the surface and move forward (in the negative x direction), as shown in Fig. 5(a). However, if the plate is dragged forward with a velocity U, the wedge will remain stationary. de Gennes equated the total viscous dissipation to the rate of surface work done to show that

$$U=\frac{\gamma\theta^3}{6\mu}\left[\ln\left|\frac{1}{\varepsilon}\right|\right]^{-1} \tag{20}$$

for small values of θ and wetting liquids. Here, $\varepsilon=\ell/L$, where ℓ is the small cutoff length (in the x direction) used in the boundary condition Eq. (14) and L is the macroscale of the problem, and equivalent to $\varepsilon=h^*/h_o$. The inverse logarithmic dependence indicates that U is insensitive to the magnitude of ε. Now, during evaporation, the contact line recedes. This has been shown schematically in Fig. 5(b). The bold line is the initial position and the dashed line is that after a time Δt. The distance between the two, as shown with the line segment perpendicular to them, is obtained from the jump balance as $(k_L p_s/\rho RT)\Delta t$, where the vapor pressure used is that away from the immediate vicinity of the contact line, where the profile is a straight line. Consequently,

$$\Delta x_o=\frac{k_L p_s}{\rho RT}\Delta t/\theta$$

is obtained. In the limit Δt goes to zero, the rate of wetting (actually the wedge is receding) is dx_o/dt. This is equated to de Gennes' velocity U with which the plate is dragged, leading to

$$\theta = \left(\frac{3\mu}{\gamma}\frac{k_L p_s}{\rho RT}\right)^{1/4}\left[\ln\left|\frac{1}{\varepsilon}\right|\right]^{1/4}, \tag{21}$$

a result that is independent of slit width. For the physical properties used here, $\theta = 2.1°$ for both cases, a result very close to those obtained from the numerical solutions discussed earlier. The importance of capillary flow on pinning is clear from the above. It is likely that its impact is lessened in nonwetting liquids and when the evaporation is nonisothermal.

We show in Fig. 6 the enhancement in the local flux over the value of $k_L p_s/RT$. This enhancement is $E = (k_L p_s'/RT)/(k_L p_s/RT)$, which is the ratio between the local flux when the effect of curvature and disjoining pressure are included and that when there are ignored. This is further generalized to take into account that the activity of the liquid is lowered in presence of the polymer by a factor of $(1-\phi)$, where ϕ varies with film thickness due to volume restriction given by the exponential factor described after Eq. (2). In particular, ϕ is ϕ_∞ when the volume restriction is not used. Consequently,

$$E = \frac{k_L p_s'(1-\phi)/RT}{k_L p_s(1-\phi_\infty)/RT},$$

where the numerator is the actual local flux and the denominator is the flux where none of the special features of thin films is included. Simplifying after using Eq. (12),

$$E = \frac{\exp\left\{-\frac{1}{RT\rho_L}\left(\gamma\frac{\partial^2 h}{\partial x^2} + \Pi\right)\right\}(1-\phi_\infty \cdot e^{-N(b/h)^{5/3}})}{(1-\phi_\infty)} \tag{22}$$

is obtained. Of course, if there is no polymer, ϕ_∞ is zero.

The plots of E in Figs. 6(a) and 6(b) dip as the contact line is approached, both because of thinning, which increases the disjoining pressure, and because of increasing curvatures. This is followed by a short rise, which is the expected rise in flux near the contact line, as explained in Sec. I. This has been suppressed because of the fall in vapor pressure, but the evaporation rate rises soon after. The cutoff prevents us from reaching the last stage where this rise is followed by a quick fall to zero. That is, the effects of changes in saturation pressure [Eq. (12)] overshadows the rise in evaporation rate that is conventionally calculated, except in a narrow range in the middle. Figure 6(c) includes the effects of polymer in form of a factor $(1-\phi)/(1-\phi_\infty)$, where ϕ goes to zero as the film thickness goes to zero;[12] that is, Fig. 6(c) differs from Figs. 6(a) and 6(b) mainly because of this term. The polymer gets excluded from the thin film region in a manner that is more marked in Fig. 6(c) because the starting thickness is a low 25 nm. These effects are lot less marked when the starting thickness is 100 nm; the case is not shown here. In Fig. 6(c) there is a fall and a rise in the rate of evaporation, just as seen in Figs. 6(a) and 6(b), but it is lot less marked.

Experimental observations have been made using nonwetting drops.[20–23] Due to evaporation, the contact angles fall below their equilibrium values, which leads the contact line to recede. The Marangoni effect pushes it forward and the contact angle is pinned. Wetting liquids treated here are quite different because the contact angles cannot fall below the equilibrium value of zero. In addition, most drops studied are water drops, which have a large latent heat, and upon evaporation should give rise to Marangoni flow. It is emphasized that when the liquids with low latent heats are used, very different observations are made as to where the contact lines recede and contact angles remain at their equilibrium

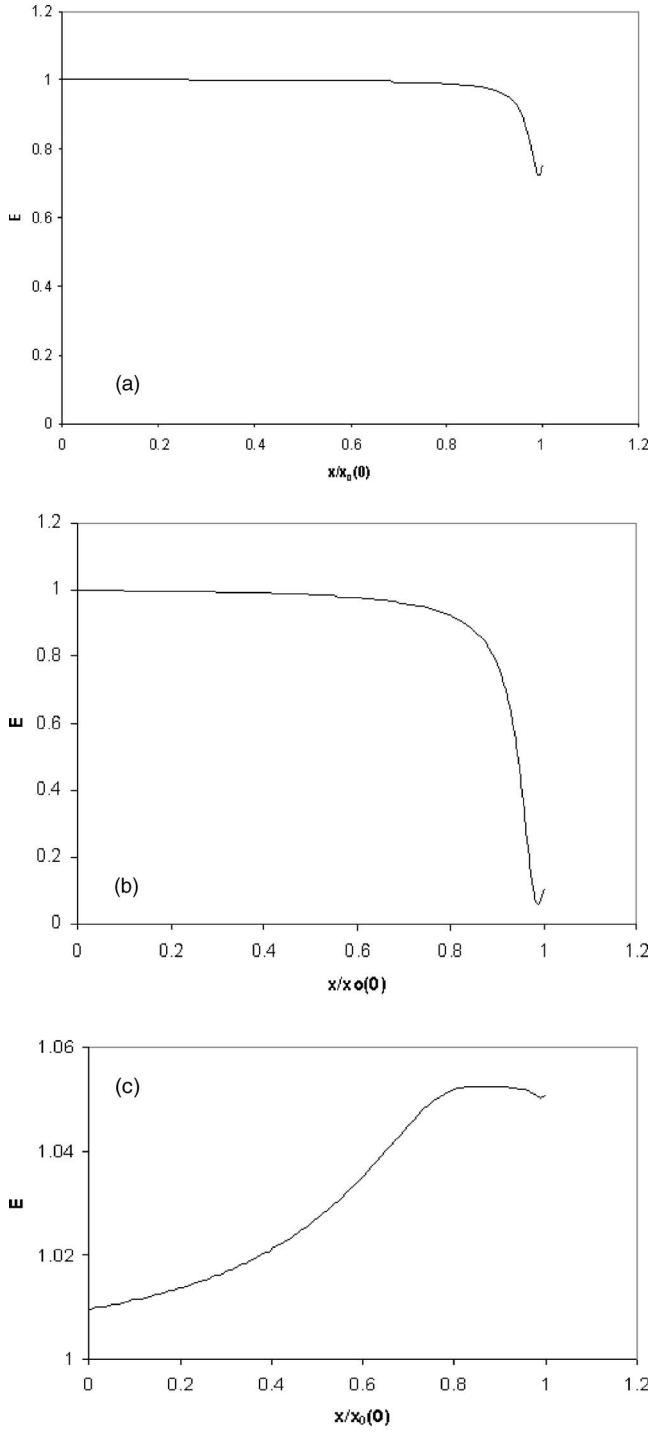

FIG. 6. Enhancement of the flux over $k_L p_s$ along the length are shown. In (a) and (b) without the polymer at $h_o = 100$ and 25 nm, respectively. (c) Polymer is included with $h_o = 25$ nm. The increase in fluxes is due to the added factor of $(1-\phi)/(1-\phi_\infty)$. The remaining case of 100 nm with polymer is less marked but similar to (c).

values.[20,23] A large section of systems therefore exists where the present considerations apply and bring in features not encountered before.

ACKNOWLEDGMENTS

This material is based on work supported by the National Science Foundation under Grant No. CTS-0228834.

[1] R. D. Deegan, O. Bakajin, T. E. Dupont, G. Huber, S. R. Nagal, and T. A. Witten, "Contact line deposits in an evaporating drop," Phys. Rev. E **62**, 756 (2000).
[2] R. D. Deegan, O. Bakajin, T. E. Dupont, G. Huber, S. R. Nagal, and T. A. Witten, "Capillary flow as the cause of ring stains from dried liquid drops," Nature (London) **389**, 827 (1997).
[3] H. Hu and R. G. Larson, "Evaporation of a sessile droplet on a substrate," J. Phys. Chem. B **106**, 1334 (2002).
[4] H. Hu and R. G. Larson, "Analysis of the microfluid flow in an evaporating sessile droplet," Langmuir **21**, 3963 (2005).
[5] H. Hu and R. G. Larson, "Analysis of the effects of Marangoni stresses on the microflow in an evaporating sessile droplet," Langmuir **21**, 3972 (2005).
[6] F. J. Renk and P. C. Wayner, Jr., "An evaporating ethanol meniscus," J. Heat Transfer **101**, 55 (1979).
[7] S. Moosman and G. M. Homsy, "Evaporating menisci of wetting fluids," J. Colloid Interface Sci. **73**, 212 (1980).
[8] P. C. Wayner, Jr., "The effect of interfacial mass transport on flow in thin liquid films," Colloids Surf. **52**, 71 (1991).
[9] A. Oron, S. H. Davis, and S. G. Bankoff, "Long-scale evolution of thin liquid films," Rev. Mod. Phys. **69**, 931 (1997).
[10] S. J. S. Morris, "A phenomenological model for the contact region of an evaporating meniscus on a superheated slab," J. Fluid Mech. **411**, 59 (2000).
[11] H. J. Palmer, "Comments on 'Insoluble monolayers and the evaporation coefficient of water' by G. T Barnes," J. Colloid Interface Sci. **65**, 574 (1978).
[12] S. Saritha, X. Zhang, and P. Neogi, "Wetting kinetics of films containing non-adsorbing polymers," J. Chem. Phys. **122**, 244711 (2005).
[13] B. V. Derjaguin, "The theory of capillary condensation and other capillary phenomena considering the disjoining action of semimolecular liquid surfaces," Zh. Fiz. Khim. **14**, 137 (1940).
[14] A. Frumkin, "Phenomena of wetting and adhesion of bubbles. I," Zh. Fiz. Khim. **12**, 337 (1938).
[15] R. M. Ybarra, P. Neogi, and J. M. D. MacElroy, "Osmotic stresses and wetting by polymer additives," Ind. Eng. Chem. Res. **37**, 427 (1998).
[16] X. Zhang, S. Saritha, and P. Neogi, "Wetting kinetics of a thin film on a solid surface pinned to a slot," Ind. Eng. Chem. Res. **44**, 1204 (2005).
[17] V. S. Ajaev, "Spreading of thin volatile liquid droplets on uniformly heated surfaces," J. Fluid Mech. **528**, 279 (2005).
[18] V. S. Ajaev and G. S. Homsy, "Three-dimensional steady state vapor bubbles in rectangular channels," J. Colloid Interface Sci. **244**, 180 (2001).
[19] P. G. de Gennes, "The dynamics of a spreading droplet." C. R. Acad. Sci., Ser. II: Mec., Phys., Chim., Sci. Terre Univers **298**, 111 (1984).
[20] C. Bourgès-Monnier and M. E. R. Shanahan, "Influence of evaporation on contact angle," Langmuir **11**, 2820 (1995).
[21] S. K. Barthwal, A. K. Panwar, and S. Ray, "Dynamic evolution of contact angle on solid substrates during evolution," in *Contact Angle, Wettability and Adhesion*, Vol. 3, edited by K. L. Mittal (VSP, Utrecht, 2003), p. 175.
[22] A. K. Panwar, S. K. Barthwal, and S. Ray, "Effect of evaporation on the contact angle of a sessile drop on solid substrates," J. Adhes. Sci. Technol. **17**, 1321 (2003).
[23] H. Y. Erbil, G. McHale, and M. I. Newton, "Drop evaporation on solid surfaces: Constant contact angle mode," Langmuir **18**, 2636 (2002).